Chapter 17

The Limits of Turning Control in Flying Insects

Fritz-Olaf Lehmann

Abstract This chapter provides insights into the turning flight of insects, considering this specific behavior from experimental and numerical perspectives. The presented analyses emphasize the need for a comparative approach to flight control that links an insect's maneuverability with the physical properties of its body, the properties and response delays of the sensory organs, and the precision with which the muscular system controls the movements of the wings.

In particular, the chapter focuses on the trade-off between lift production and the requirement to produce lateral forces during turning flight. Such information will be useful not only for a better understanding of the evolution and mechanics of insect flight but also for engineers who aim to improve the performance of the future generation of biomimetic micro-air vehicles.

17.1 Introduction

Insects display an impressive diversity of flight techniques such as effective gliding, powerful ascending flight, low-speed maneuvering, hovering, and sudden flight turns [1–9]. Flies, in particular, are capable of extraordinary aerial behaviors aided by an array of unique sensory specializations including neural superposition eyes and gyroscopic halteres [10–12]. Using such elaborate sensory input, flies steer and maneuver by changing many aspects of wing kinematics including angle of attack, the amplitude and frequency of wing stroke, and the timing and speed of wing rotation [13–18]. The *limits* of these kinematic alterations, and thus the constraints on the aerial maneuverability of a fly, depend on several key factors including the maximum power output of the flight muscles, mechanical constraints of the thoracic exoskeleton, and the ability of the underlying neuromuscular system to precisely control wing movements [19–22].

What we experience as flight behavior of a flying insect reflects the output of a complex feedback cascade that consists of receptors to collect sensory information, the central nervous system and thoracic ganglion to process this information and to produce locomotor commands, and the mechano-muscular system to drive the wings (see also Chaps. 1– 7). Changes in flight behavior result from changes in any of these components such as alterations in the sensory input or in the bilateral symmetry of flight force production caused by wing damage. Due to the predominant role of the compound eyes for navigation, orientation, and flight stability, the vast majority of investigations on flight control in the past have been done on the question of how changes in the visual input change aerial behavior and thus on the question of how the nervous system processes visual information [23–31].

Flight control and maneuverability of flies have been studied by a variety of methods under both free and tethered flight conditions. Although tethered flight reflects only a small fraction of an insect's total behavioral repertoire in free flight, this technique has proven useful in elucidating the organization of the flight control system in flies such as optomotor behaviors in response to rotating and expanding visual flow fields and object orientation behaviors [32–39]. A major

F.-O. Lehmann (✉)
Institute of Neurobiology, University of Ulm,
Albert-Einstein-Allee 11, 89081 Ulm
e-mail: fritz.lehmann@uni-ulm.de

D. Floreano et al. (eds.), *Flying Insects and Robots*,
DOI 10.1007/978-3-540-89393-6_17,

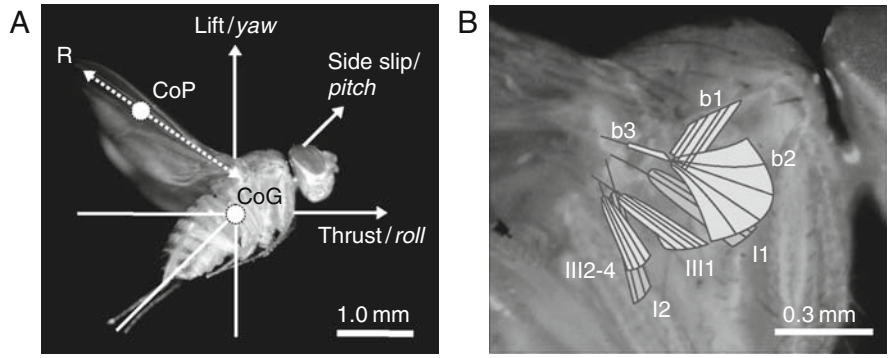

Fig. 17.1 Free flight body posture and flight muscles in the 1.2 mg fruit fly *Drosophila*. (**A**) Rotational axes and forces, (**B**) subset of the 17 pairs of flight control muscles involved in amplitude control for yaw turning. Neural activation of the basalare b1–b3 causes an increase in stroke amplitude. Muscle spikes in the first (I1–I2) and third (III1–III4) pterale typically result in a decrease in amplitude. R, wing length; CoP, aerodynamic center of pressure on wing; CoG, the fly's center of gravity

disadvantage of tethered studies, however, is the lack of adequate feedback from sensory organs such as the halteres and the antennae. Moreover, tethered flight studies in flight simulators require elaborate computational algorithms for feedback simulation, in order to model the physical behavior of the insect body similar to what would occur in free flight. Thus, despite the difficulty in reconstructing body and wing motion in freely flying animals and in assessing sensory stimuli, free flight measurements are crucial because they capture the behavior of an animal in a more natural context and under natural closed-loop feedback conditions between the fly's sensory and motor system. Besides the control for adjusting translational forces such as thrust and body lift, yaw turning during maneuvering flight has attracted considerable interest, because it determines flight heading and is thus of augmented ecological relevance for foraging behavior and search strategies in an insect.

This chapter attempts to summarize some of the most important factors for yaw turning control in an insect, such as the time course of yaw torque production and thus the temporal changes in wing motion, the constraints on sensory feedback, and the physics of turning. The chapter especially highlights the significance of the ratio between the body mass moment of inertia and the frictional damping between the body structures and the surrounding air. Experimental results and numerical predictions will further demonstrate some of the most important trade-offs in flight control and also show how the maximum locomotor capacity constrains stability and maneuverability at elevated muscle mechanical power output during flight of the small fruit fly *Drosophila melanogaster* (Fig. 17.1).

17.2 Free Flight Behavior and Yaw Turning

In many insects, including the fruit fly, straight flight in a stationary visual environment is interspersed by sudden flight turns termed *flight saccades*. Flight saccades are maneuvers in which the fruit fly quickly changes flight heading between 90° and 120° within 15–25 wing strokes (75–125 ms, Figs. 17.2 and 17.3) [3, 5, 7]. Due to their high dynamics, these maneuvers differ from other forms of turning flight such as continuous, smooth turning behavior with angular velocities well below 1000° s^{-1}. There is an ongoing debate on the exact angular velocity profile during saccadic turning, because this profile critically depends on at least three factors: the time course of yaw torque production, the moments of body inertia, and the frictional damping on body and wings [40]. Although the maximum angular velocity of approximately 1600° s^{-1} within a saccade is independent of the forward speed in fruit flies, flight saccades are supposedly not uniform maneuvers in terms of a fixed motor action pattern. Instead, measurements have shown that the total turning angle within a flight saccade varies between 120° and 150°, potentially depending on the visual input the animals have experienced prior to the turn [40].

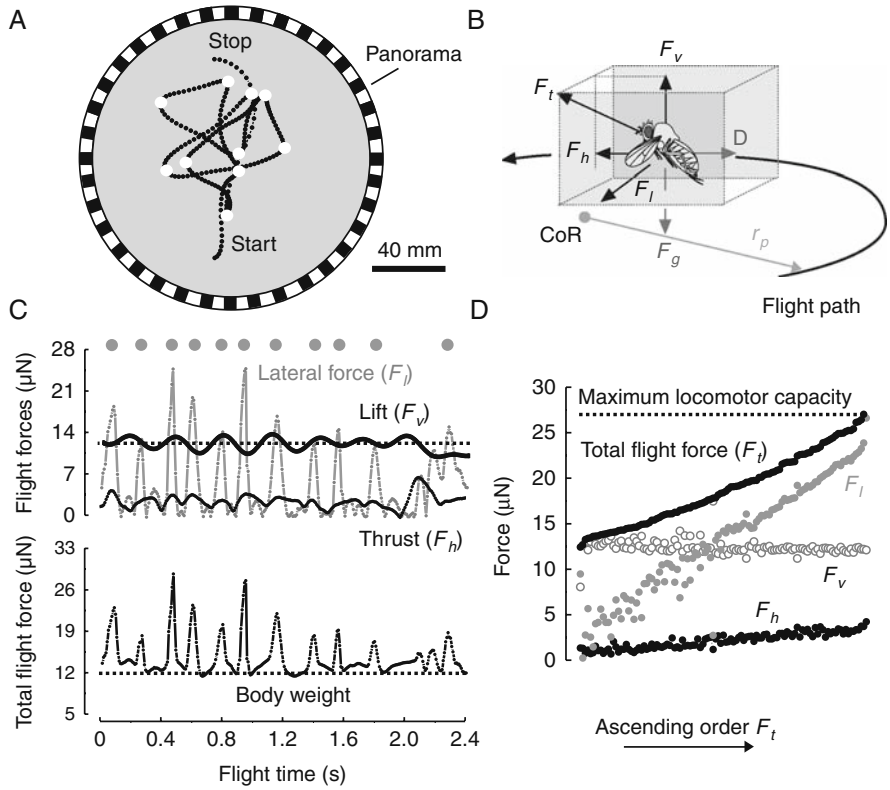

Fig. 17.2 Flight behavior and forces in freely flying fruit flies. (**A**) Saccades (*white dots*) of a 2.4 s flight path within a cylindrical, 170 mm high, free flight arena surrounded by a random-dot visual panorama. Sample time = 8 ms. (**B**) Forces during flight, (**C**) time traces of forces acting on the animal (*upper traces*) and total flight force production (*lower trace*). *Gray dots* indicate the times at which saccades occur in (**A**). (**D**) Total force and ratio between force components within flight recordings that fell within the top 10% maximum of total force. F_v, vertical force (lift); F_l, lateral force (centripetal); F_h, horizontal force (thrust); F_t, total force; F_g, gravitational force. D, body drag; r_p, flight path radius; CoR, center of radius

A potential threat on an animal during fast yaw turning at elevated forward velocity is the occurrence of centrifugal forces that cause side-slip motion [41]. Drifting during turning is a serious problem when the insect must quickly change its flight course, for example, in response to an approaching obstacle. Besides the centering response, obstacle avoidance behavior is of great ecological significance because it allows an insect to safely cruise through dense vegetation and also to escape from predators [42, 43]. Thus, to avoid sideslipping and to stay on track within the saccade, insects must compensate for centrifugal forces by producing centripetal forces. Many insects achieve this behavior by performing bank (roll) turns,

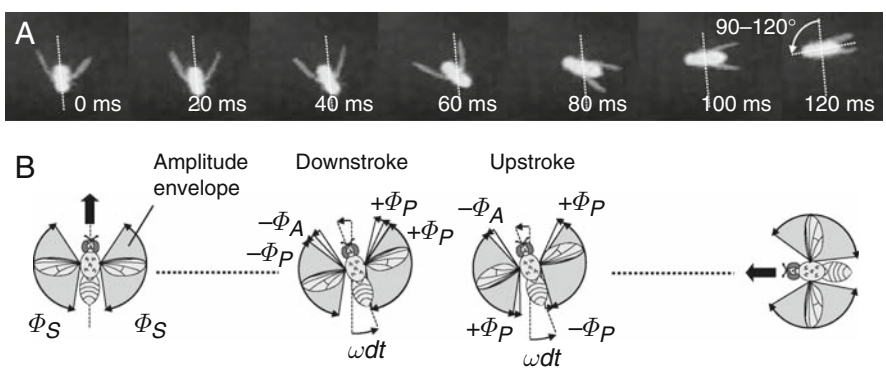

Fig. 17.3 Free flight saccade visualized by high-speed video. (**A**) Images (*top view*) show body orientation and wing position at ventral (0–60 ms) and dorsal (80–120 ms) stroke reversals. (**B**) Mean stroke amplitude (Φ_S) supports body weight. Changes in stroke amplitude on each body side result from passive components (Φ_P) due to body rotation and active components (Φ_A) due to changes in the activity of flight control muscles. Cycling period of a stroke cycle is ~5 ms (200 Hz)

in which the mean flight force vector tilts sideways, toward the inner side of the flight curve [44]. In fruit flies, side-slipping movements are rare, and even at their maximum forward velocity of 1.22 ms^{-1} the animals are apparently able to completely compensate for centrifugal forces while turning [5]. In terms of total force balance, lateral force production is of particular significance, because in the fruit fly the production of centripetal forces consumes up to 70% of the locomotor reserves [5, 19, 22].

17.3 Forces and Moments During Turning Flight

The physical parameters predominantly determining changes in forward-, upward-, and side-slip velocities of an insect are the frictional damping coefficient on body and wings and body inertia [3, 40]. Turning rate, by contrast, is determined by the frictional damping coefficient and the mass moment of inertia of the body. The former measure determines air friction during body motion, where a higher frictional damping coefficient results in a lower peak turning velocity at constant torque production. Mass moment of inertia, in turn, determines how quickly the animal may alter its angular velocity around the three vertical and horizontal body axes: yaw, pitch, and roll (Fig. 17.1A). Elevated inertia, moment of inertia, and frictional damping potentially favor stable flight because these factors reduce angular and translational accelerations (inertia) and also maximum angular and translational velocities (friction) in an insect. A major benefit of passive frictional damping is that it reduces the computational load needed to process sensory feedback signals by the nervous system and decreases the required precision for wing control (see Sect. 17.4.2.3). The benefit of frictional damping for flight stabilization is also shown in birds [45]. For example, wing-based damping in wing amplitude asymmetry-driven turning is an important mechanism for roll dynamics during aerodynamic reorientation, because the roll damping coefficient in cockatiels is two to six times greater than the coefficient typical of airplane flight dynamics [45]. However, high moment of inertia and frictional damping also limit flight agility [1−9]. Flight behavior is thus a compromise between the need to stabilize the animal body and the need to allow quick maneuvers, for example, in order to escape from predation or to avoid collisions with nearby objects in the environment.

17.3.1 Modeling Friction and Moment of Inertia

In general, an insect's instantaneous angular velocity during yaw turning ω at a given time t results from the three major components: the torque T produced around the vertical body axis, the moment of inertia I given by the body mass distribution of the animal, and the frictional damping coefficient C of body and wings [3, 40]. This relationship thus becomes

$$T(t) = I\dot{\omega}(t) + C\omega(t). \tag{17.1}$$

A rough estimate of the moment of inertia may be derived when assuming that the shape of the insect body can be approximated by a long thin cylinder with a given length l that rotates around its vertical axis at 50% length (Fig. 17.1A). Inserting body length and body mass m_b, the moment of inertia of an insect may be easily derived from the simple equation

$$I = \frac{m_b l^2}{12}. \tag{17.2}$$

Both the mass moment of inertia and the frictional damping coefficient C_B of such a cylinder are relatively small; in the fruit fly the two measures yield only 0.52 $pNms^2$ and 0.52 pNms, respectively.

By contrast, the wings' contribution to friction during yaw rotation is more complicated because this measure depends on the complex aerodynamics of the flapping wings. In general terms, frictional damping due to flapping wings depends on the differences in profile drag between the up- and downstroke and the left and right wing. Drag, in turn, depends on stroke frequency, amplitude, the ratio between up- and downstroke, wing length, mean drag coefficient, and also on the location of the center of pressure on each wing (Fig. 17.1A). The combined damping coefficient for an insect is the sum of wing-based damping and body damping C_B, and we can write this sum as

$$C = \frac{\bar{D}_{Dif}\hat{r}_{CP}\,(R + 0.5\,W)}{\bar{\omega}} + C_B, \qquad (17.3)$$

in which the numerator is equal to the frictional moment given by the product between mean difference in profile drag between the two wings $\bar{D}_{Dif}$ and the length of the moment arm, where R is wing length, W is thorax width, and $\hat{r}_{CP}$ is the relative location to the wing's center of pressure [40]. The dominator is mean angular velocity during turning.

Deriving $\bar{D}_{Dif}$ is challenging, because this measure depends on wing velocity in each half stroke. Mean wing velocity is proportional to the product between stroke frequency and stroke amplitude. The latter measure, however, changes during turning due to two processes: first, passively in the global coordinate system, as the result of body rotation, and second, actively as a result of the bilateral difference in wing beat amplitude used for yaw torque production (Fig. 17.3). Experiments in both tethered animals flying in a reality flight simulator and in free flight show that during counterclockwise (clockwise) turning flies increase (decrease) its wing beat amplitude on the right body side and decrease (increase) the amplitude on the left side (Fig. 17.4A).

The first step in deriving the damping coefficient for yaw turning is thus to derive wing velocity in each half stroke. According to Ellington, the mean wing velocity of a wing segment in each half stroke $\bar{u}(r)$ at normalized distance r (0–1) from the wing base is proportional to the product between dimensionless wing velocity, the dimensionless wing velocity profile during up- and downstroke $d\hat{\phi}/d\hat{t}$, stroke frequency, mean stroke amplitude Φ_S, and wing length R [46]. Assuming that both the dimensionless velocity profile and stroke frequency remain constant during turning and

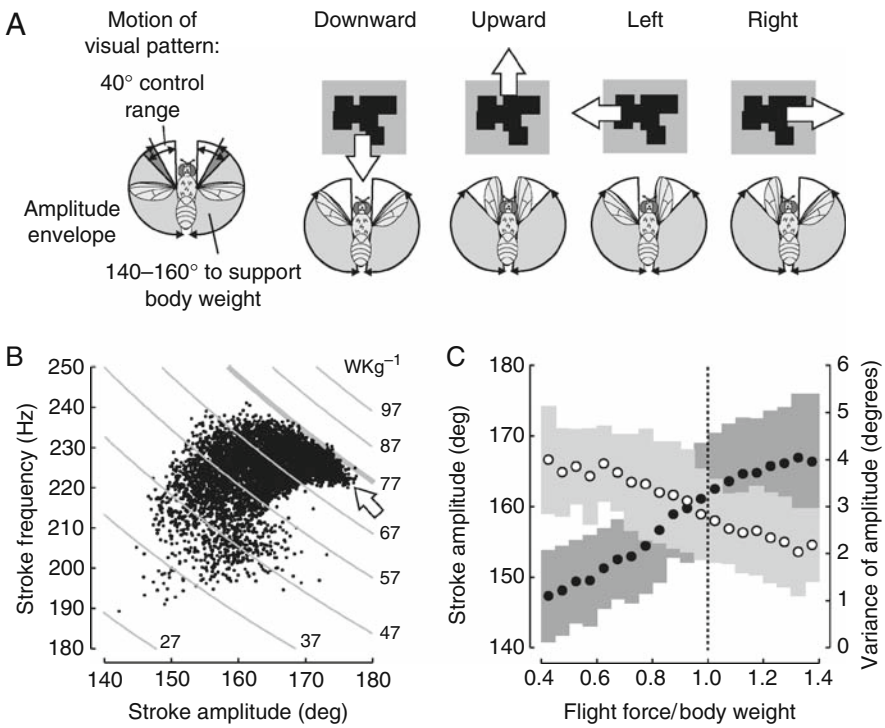

Fig. 17.4 Stroke amplitude control by tethered fruit flies flying inside a virtual reality flight simulator. (**A**) The flies try to compensate for the motion of the visual panorama displayed inside the arena by actively modulating its stroke amplitude. (**B**) In vivo working range (kinematic envelope) of a tethered fruit fly responding to visual stimulation while actively controlling the azimuth velocity of the visual panorama using the bilateral difference between left and right stroke amplitude. At maximum flight force production (*arrow*), the control of moments is compromised because the animal is restricted to a unique combination between stroke amplitude and frequency [50]. Hyperbolic lines represent mechanical power isolines of the indirect flight muscle [22]. (**C**) Mean stroke amplitude (*closed circle*) and temporal variance (*open circle*) of *left* and *right* stroke amplitudes plotted against relative flight force production. *Gray* areas indicate standard deviations

only stroke amplitude changes due to passive Φ_P rotation of the animal body and active steering Φ_A, the velocity at the wing's center of pressure and for a half stroke can be written as

$$\bar{u} = \tfrac{1}{2}\overline{|d\hat{\phi}/d\hat{t}|}\,(\Phi_S + \Phi_P + \Phi_A)\,\frac{n}{j}\hat{r}_{CP}R. \qquad (17.4)$$

Due to the bilateral symmetry between left and right wing and the ratio between up- and downstroke, passive and active amplitudes have different signs in each half stroke (Fig. 17.3). If we consider a counterclockwise turn of the animal, Φ_P is positive for the left (right) wing during the up (down)stroke and negative during the down (up)stroke (Fig. 17.3B). Since a counterclockwise turn requires an increase in stroke amplitude on the right body side and a decrease on the left side, the active component Φ_A is negative (positive) in the left (right) wing in both half strokes. Another modification in the above equation is the effective frequency in each half stroke that depends on the time periods of up- and downstroke. Effective frequency is the ratio between stroke frequency and relative time spent during the up- and downstroke ($\hat{t}$ = fraction of downstroke in a complete stroke cycle {0–1}). Thus, the parameter j in the above equation is equal to $\hat{t}$ during the downstroke and amounts to $1 - \hat{t}$ during the upstroke.

In a second step, we employ a numerical model that converts velocity estimates into mean wing profile drag $\bar{D}$. The most simple approach to derive $\bar{D}$ for each wing is to use Ellington's 2D quasi-steady aerodynamic model based on wing velocity squared and to lump unsteady aerodynamic effects, such as the development of a leading edge vortex, together into a mean drag coefficient [5, 46]. Despite ignoring 3D flow conditions, modified versions of this approach have successfully been used in insect flight research (for *Drosophila* see [18]). By combining the various velocity estimates with the quasi-steady model, we may derive the desired drag residual during turning from the differences in drag between left and right wing within the entire stroke cycle, whereby drag is positive during the downstroke and negative during the upstroke. We finally get the following expression:

$$\bar{D}_{Dif} = \frac{1}{2}\rho\bar{C}_{D,Pro}S\left(\hat{t}\bar{u}^2_{L,D} + \left(1-\hat{t}\right)\bar{u}^2_{R,U} - \left(1-\hat{t}\right)\bar{u}^2_{L,U} - \hat{t}\bar{u}^2_{R,D}\right), \qquad (17.5)$$

Table 17.1 Description of modeling parameters for the fruit fly [40]

Symbol	Description	Value
Φ_S	Wing stroke amplitude for weight support	140° (2.44 rad)
N	Wing stroke frequency	218 Hz
$\bar{\omega}$	Saccadic turning rate	1600° s^{-1} (27.9 rad s^{-1})
$\hat{t}$	Relative duration of downstroke	0.538
$\Phi_{P,U}$	Passive wing stroke difference upstroke	4.0° (0.069 rad)
$\Phi_{P,D}$	Passive wing stroke difference downstroke	3.1° (0.054 rad)
Φ_A	Mean active wing stroke difference	5° (0.087 rad)
$\hat{r}_{CP}$	Normalized distance to center of pressure	0.7
R	Wing length	2.47×10^{-3} m
W	Thorax width	1.0×10^{-3} m
P	Density of air	1.2 kg m^{-3}
$\bar{C}_{D,Pro}$	Mean profile drag coefficient of wing	1.46
S	Surface area of one wing	2.0×10^{-6} m^2
$\overline{\lvert d\hat{\phi}/d\hat{t}\rvert}$	Dimensionless wing velocity	4.4

where $\bar{u}_{L,D}(\bar{u}_{R,D})$ and $\bar{u}_{L,U}(\bar{u}_{R,U})$ are wing velocities for the down- and upstroke of the left (right) wing, respectively (see Table 17.1 for abbreviations).

17.3.2 The Consequences of High Frictional Damping

The ratio between moment of inertia and aerodynamic damping (I/C) is a critical measure for the control of body dynamics by the neuromuscular system of an insect. At high ratio when flight is dominated by the forces due to the distribution of body mass, turning acceleration is low but turning rate steadily increases when the animal produces rotational moments. At low ratio, by contrast, angular acceleration is high but angular velocity saturates with increasing turning rate [40]. These relationships have two consequences: Insects with an elevated moment of body inertia compared to frictional damping potentially benefit from an increase in flight-heading stability, but may lose control at high turning rates at which the transfer function

of the sensory structures becomes highly non-linear. Moreover, once the animal has initiated yaw moments, turning rate decreases only slowly when torque production vanishes. In this case, an insect must actively brake in order to terminate its turning by producing counter torque as shown in Fig. 17.5B.

By contrast, small insects such as fruit flies that rely on relatively low *I*/*C* ratios are comparatively unstable around their rotational axes because their angular acceleration is high at low torque production [40]. These insects need to have a precise flight apparatus by allowing either a higher spatial resolution in wing amplitude control and other kinematic parameters, or a higher temporal resolution by decreasing the lack in response time of sensory feedback. High damping, however, allows an animal to passively terminate its turn without applying any kind of counter torque. In insects flying at relatively high damping coefficients,

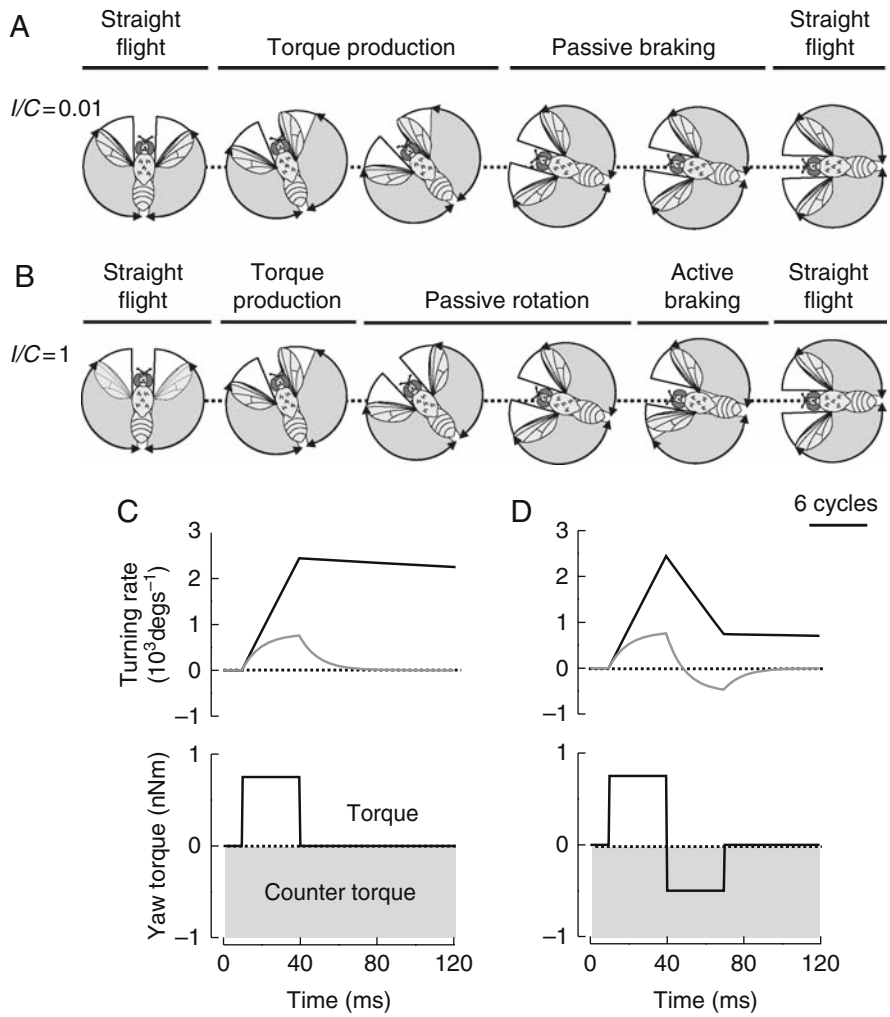

Fig. 17.5 Numerical modeling of yaw turning at two ratios between mass moment of inertia and frictional damping (*I*/*C*) on body and wings [40]. (**A**) Changes in stroke amplitude at small *I*/*C* ratio, corresponding to what is predicted for the fruit fly. (**B**) The fly must actively terminate yaw turning (counter torque) at high *I*/*C* ratio when frictional damping is considered on the body alone [3]. (**C**) Turning rates at low (*black*) and high (*gray*) frictional damping (cf. *A* and *B*) in response to a single 30 ms 0.8 pNms yaw torque pulse in the fruit fly. (**D**) Counter torque at the end of the saccade (*lower graph*) produces negative turning rates when the model includes frictional damping on wings (*gray, upper graph*). Without frictional damping (*black, upper graph*), the production of counter torque reduces turning rate but does not totally terminate saccadic rotation. Values for the fruit fly are $I = 0.52$ pNms^2; $C = 0.52$ and 54 pNms for body damping alone (in *B*) and combined frictional damping on body and wings (in *A*), respectively

the production of high counter torque might even partly annihilate directional changes initiated at the beginning of the flight turn (Fig. 17.5D).

When inserting the values of Table 17.1 for the fruit fly into the numerical model (Eq. 17.5), we obtain a total frictional damping coefficient C of 54 pNms due to the flapping wings that is approximately 100 times the value estimated from the body alone (0.52 pNms). Combining all estimates of moment of inertia, torque production, and damping in the fruit fly, the damping term in torque equation (17.1) is roughly 4–16 times larger than the inertia term. This finding is also confirmed by an elaborate 3D computational fluid dynamic (CFD) study on *Drosophila* yaw turning [47], suggesting a CFD torque profile similar to that shown in Fig. 17.6B (no active braking), rather than to a biphasic torque profile that includes active braking [3]. Consequently, in fruit flies friction plays a larger role for yaw turning behavior than moment of inertia.

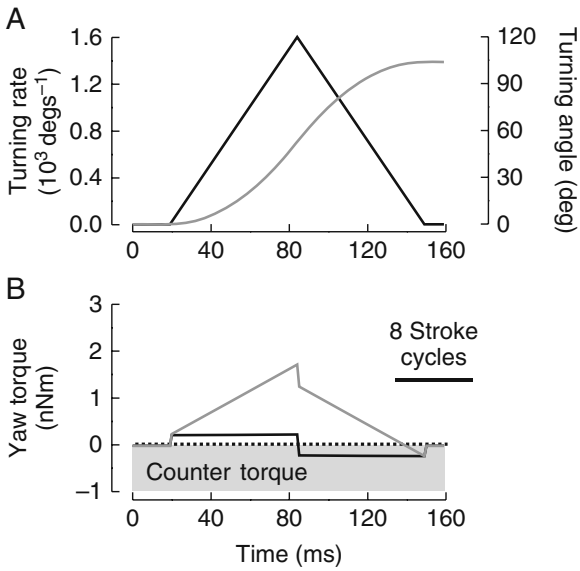

Fig. 17.6 Modeling of yaw torque during a saccadic turn of a freely flying fruit fly. (**A**) Torque development is calculated using a simplified velocity profile of turning rate (*black*) and turning angle (*gray*), measured in freely flying flies (cf. Fig. 17.2A) [5]. (**B**) At its natural frictional damping coefficient of 54 pNms on body and wings, the fruit fly does not depend on active braking (i.e., the production of counter torque) to terminate the saccade (*gray line*). Assuming damping on the fly body alone (1% of wing damping coefficient), however, active braking is required to terminate the saccade (*black*)

17.4 Balancing Aerodynamic Forces During Maneuvering Flight

Based on the assumption that flight in fruit flies is dominated by frictional forces rather than by inertia, the forces acting on the fly body during maneuvering flight may be derived from a simple numerical model for force balance. The development of such a model is beneficial for several reasons: First, it gives insight into how total aerodynamic forces are distributed among horizontal-, vertical-, and lateral components; second, it allows predictions of the relationship between flight path curvature and forward velocity; and third, it allows estimations of the maximum locomotor capacity in a freely flying animal. The following sections describe the various force components required for flight and show how force and velocity components may be determined in a freely cruising animal.

17.4.1 Forces and Velocities

Flight velocity and thus flight direction of an insect depends on the ratio between vertical force (body lift), horizontal force (thrust), and lateral force (sideslip) multiplied by normalized friction and on the moments around these vectors: yaw (vertical axis), roll (horizontal axis), and pitch (lateral axis, Fig. 17.1A). While forces for translation are considered to play a major role in force balance of the fruit fly, the forces needed to generate torque are negligible. This assumption is fostered by torque measures obtained during optomotor behavior in tethered flies flying inside a virtual reality flight arena. Under these conditions, fruit flies typically vary yaw torque by not more than ± 1.0 nNm (Fig. 17.5C,D) [48]. At a moment arm of 65% wing length from the wing base for the wing's center of pressure (equal to the center of force, Fig. 17.1A) [49], this moment requires forces of not more than 0.50 μN or approximately 3% of the maximum flight force in this animal. Thus, the production of moments around the three body axes should require only minor modification in instantaneous force production by the flapping wings.

For the above reason, we may model flight, assuming that total flight force F_t produced by both wings is equal to the vector sum between vertical-, horizontal-,

and lateral forces (F_v, F_h, and F_l, respectively), written as

$$F_T = \sqrt{F_h^2 + F_v^2 + F_l^2}. \tag{17.6}$$

To transform these forces into velocity estimates, we use a simplified approach assuming frictional damping at low Reynolds number. Reynolds number for body motion depends on forward velocity and thus varies between values close to zero at slow forward flight and, in the fruit fly, approximately 64 at maximum cruising speed (mean body width = 0.8 mm, kinematic viscosity of air = 15×10^{-6} $m^2 s^{-1}$). Although these values suggest a conventional 'force–velocity-squared' relationship, measurements on tethered flies show that flight force production is also linearly correlated with wing velocity (non-squared) given by the product between stroke amplitude and frequency (Reynolds number = 120–170) [18]. We may thus derive a reasonable approximation of forces acting on the fly body by using Stoke's law and normalized friction [40]. Consequently, to estimate maximum flight velocities at a given flight path curvature of the insect, we replace thrust in Eq. (17.6) by body drag given as the product between normalized friction on body and wings and forward speed and lift by the sum of gravitational force and drag on the fly body when moving in the vertical. Lateral force, needed to keep the animal on track during yaw turning, is equal to centrifugal force because sideslip is negligibly small in fruit flies [40]. The latter force equals the product between the path radius r_p, horizontal velocity, and body mass m_b. The three forces are then

$$F_h = k u_h, \quad F_l = m_b u_h^2 r_p^{-1}, \quad \text{and} \quad F_v = k u_v + m_b g, \tag{17.7–17.9}$$

respectively, where g is the gravitational constant. If we now replace the force terms in Eq. (17.6) by the expressions in Eqs. (17.7–17.9), *maximum* horizontal and vertical flight velocities (u_h and u_v, respectively) at various flight conditions can be derived from the following two equations:

$$u_h = \frac{1}{m_b}\sqrt{\frac{1}{2}\left(\sqrt{r_p^4 k^4 - 4 r_p^2 m_b^2 \left(F_v^2 - F_t^2\right)} - r_p^2 k^2\right)}, \tag{17.10}$$

and

$$u_v = \frac{\sqrt{F_T^2 - k u_h^2 - m_b^2 u_h^4 r_p^{-2}} - m_b g}{k}. \tag{17.11}$$

The fly's turning velocity ω is given by the product between horizontal velocity and path curvature,

$$\omega = u_h r_p^{-1}. \tag{17.12}$$

The most critical measure in these equations is normalized friction on body and wings during forward flight, because this parameter determines maximum horizontal and vertical flight velocities. In contrast to yaw turning, estimations of normalized friction for body translation are susceptible to major errors for two reasons: First, friction on the body depends on body posture which changes with flight speed as shown by David [50] and, second, the orientation of the wings continuously changes within the stroke cycle with respect to the oncoming air. It is thus advantageous to calculate normalized friction from Eq. (17.7) using an estimate of maximum forward velocity of the insect derived from behavioral experiments and an estimate for maximum thrust derived from maximum locomotor capacity. In case of the fruit fly, reconstructions of the flight path in freely flying individuals revealed a maximum horizontal velocity of approximately 1.22 m s^{-1} at level flight.

By contrast, estimations of maximum locomotor capacity of the fruit fly are more challenging. There are at least two ways to derive this measure: First, from load lifting experiments in which freely flying animals are scored on their ability to lift up small weights as shown by Marden [51], and second, from direct force measurements in tethered flies [18, 22]. In load lifting experiments, locomotor reserve and thus maximum thrust is equal to the load that the animal is able to lift up, while in tethered flight experiments maximum locomotor capacity is equal to maximum force production when the animal is stimulated under visual open-loop optomotor conditions in a flight simulator with a vertically oscillating stripe grating. For the fruit fly, both approaches yield similar estimates for maximum thrust of approximately 4.9 μN and normalized friction in *Drosophila* thus amounts to approximately 4.0 $\mu N m^{-1} s$ (Eq. 17.7).

17.4.2 Trade-Offs Between Locomotor Capacity and Control

High aerial maneuverability of a flying insect may be useful in a large variety of behavioral contexts

including predator avoidance, prey catching, mating success, and male–male competition. A well-known example of predator avoidance is, for example, the evasive flight reaction of noctuid moths when they detect the ultrasound of predating bats [52]. Stability and maneuverability are two sides of the same coin, and the system that allows high stability in an insect also controls and constrains maneuverability. The ability of an insect to provide aerodynamic forces in excess of its body weight thereby appears to be a key factor for high maneuverability. Studies, for example, on butterfly take-off behavior show that a critical measure for high aerodynamic performance is the ratio between flight muscle and body mass [53]. In other insect species, such as dragonflies, this ratio also depends on age. Young dragonflies are typically poor flyers but gain muscle mechanical power output during adult growth. Maximum power reserves for both flight force production and steering performance are exhibited at maturity. At this stage, dragonflies defend a territory, and aerial competition determines their mating success [54].

In the fruit fly, these trade-offs between power output and flight control can be predicted by a force balance model and verified by experiments under free and tethered flight conditions. In the following sections we thus focus on the relationships between muscle performance, mechanical constraints of the thorax, and flight control in the fruit fly, i.e., (1) the trade-off between lift, thrust, and lateral force production during turning flight and its consequences for flight velocity; (2) the collapse of steering envelope at maximum locomotor performance; and (3) the significance in precision, with which the neuromuscular system is able to control bilateral stroke amplitudes during yaw turning. Altogether, these issues highlight the problems and limits of maneuvering flight in the small fruit fly and also show how our numerical model (Sect. 17.4.1) may explain the various behaviors we observe in flying flies.

17.4.2.1 The Trade-Off Between Lift, Thrust, and Lateral Forces

In the previous section we learned about the relationships between forward, upward, and turning velocity and how these parameters depend on total force production. Free flight experiments in fruit flies show that the lateral force needed to keep the animal on track during a flight saccade clearly outscores thrust and lift and almost reaches 28 μN (Fig. 17.2C). Thus, short-time total flight force production even reaches 32 μN, which is approximately three times the body weight of the animal (~1.2 mg) and above the value typically measured under tethered flight conditions. By contrast, thrust only contributes moderately to total force (<14%), and vertical force even decreases with increasing locomotor output (Fig. 17.2D) [5]. Consequently, an animal that attempts to avoid sideslipping during turning flight faces a trade-off between path curvature, flight altitude, and horizontal velocity. With respect to this trade-off, the maximum locomotor capacity (in most insects approximately twice their body weight) is an important measure that does limit not only the insect's load lifting capacity but also its flight style during fast yaw turns [51].

Using the numerical framework in Eqs. (17.6, 17.7, 17.8, 17.9, 17.10, 17.11, 17.12), the above relationships may be quantified at various maximum locomotor capacities of the animal (Fig. 17.7A). Especially when performing small-radius flight turns, horizontal and vertical velocities should decrease when lateral force production increases during turning. This effect becomes most visible at elevated forward speed when a significant part of the locomotor reserves is used to produce thrust. During yaw turning, the numerical model thus predicts a break point in flight path radius at which the fly can no longer produce constant lift and thrust. In other words, there is a minimum flight path radius that the fly may achieve at constant horizontal velocity and level flight. Any decrease in radius below this threshold either results in a decrease in forward flight speed or a loss in flight altitude or both. Figure 17.7B shows that at a moderate, constant cruising speed of 0.6 ms^{-1}, fruit flies can only keep their flight altitude (zero vertical velocity) at flight path radii above approximately 50 mm. Smaller values result in a sudden and considerable loss in flight altitude.

The trade-off between the various velocities predicted from numerical models can be verified by experimental data. Similar to what has been mentioned above, trade-offs are most visible when an animal tries to maximize flight force production. In free flight, this can be achieved by optomotor stimulation using a random-dot visual panorama that rotates at high angular velocity around the animal (>900° s^{-1}, Fig. 17.2A). In response to this visual stimulation, fruit flies typically minimize the retinal slip on their compound eyes

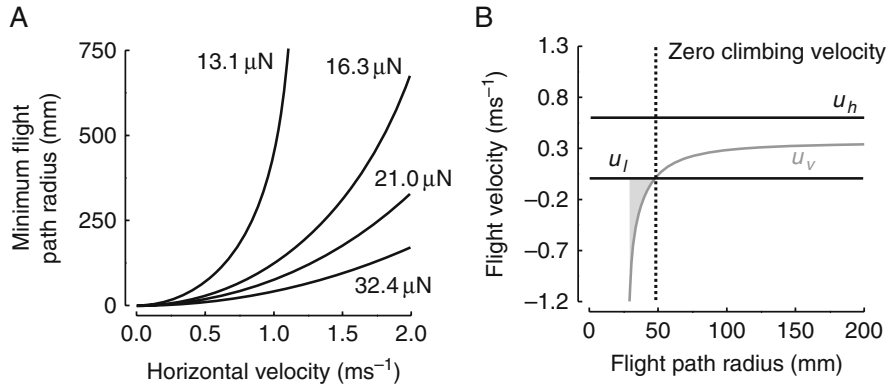

Fig. 17.7 Numerical modeling of force balance in freely flying fruit flies. (**A**) Minimum flight path radius at a given forward velocity and level flight shown for four estimates of total flight force. Maximum flight forces are 16.3, 21.0, and 32.4 μN in tethered flight, load lifting free flight, and free flight under optomotor stimulation, respectively. (**B**) Alteration in maximum vertical climbing velocity (u_v) at a mean forward cruising speed (u_h) of 0.6 ms^{-1} and assuming 16 μN maximum flight force. *Gray* area indicates path radii at which the fly loses flight altitude while turning. Lateral speed (u_l) is equal to zero because of side-slip compensation

similar to what has been observed in tethered flies [16, 31, 32, 34, 35]. Consequently, in the attempt to match forward velocity to translational velocity and turning rate to angular velocity of the rotating visual environment, the animals continuously move in concentric circles around the arena center [5]. Under these conditions, the flies' vertical speed approaches zero (constant altitude) while forward velocity and turning rate typically vary out-of-phase (Fig. 17.8). The numerical model in Eq. (17.6) predicts this behavior because at maximum locomotor capacity and constant flight altitude, any increase in lateral force production should lead to a corresponding decrease in thrust.

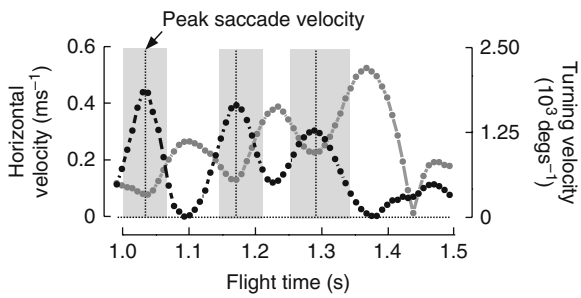

Fig. 17.8 Trade-off between horizontal velocity (*gray, left scale*) and turning velocity (*black, right scale*) in a freely flying fruit fly at elevated flight force production. Horizontal velocity and turning rate co-vary during saccadic turning (*gray areas*) presumably due to the production of elevated centripetal forces

Moreover, since an increase in total flight force requires an increase in mechanical power output of the asynchronous flight musculature, transgenic flies with reduced muscle mechanical power output exhibit larger flight path radii during turning than wild-type animals flying at similar forward speed. We noticed this behavior in a myosin light chain mutant (*MLC*2) and several fly lines in which the phosphorylation capacity of the muscle protein flightin (*fln*) had been modified by point mutation (F.-O. Lehmann, unpublished data) [55]. Flightin is a multiply phosphorylated myosin-binding protein found specifically in indirect flight muscles (IFM) of *Drosophila*. When flown in a flight simulator and scored on maximum locomotor capacity, both strains show reductions in stroke frequency and partly also in stroke amplitude, whereas muscle and aerodynamic efficiency are similar among the two transgenic strains and wild type files.

17.4.2.2 Collapse of Steering Envelope at Maximum Locomotor Performance

Since propulsion and control reside in the same locomotor system, flight control in insects is constrained by the mechanical limits of the thoracic exoskeleton that generates wing motion. The relationship between propulsion and control is of fundamental consequence because it predicts a complete loss in control at maximum locomotor force production. In general,

locomotor reserves of an insect function as power reserves to boost horizontal or vertical flight velocities but also allow the insect to *modulate* wing kinematics. Since many insects control lift and yaw moments by changing stroke amplitude (not dragonflies that apparently more often use changes in angle of attack and wing phasing for steering) [1, 8, 56–60], flying with amplitudes near the mechanical limits should impair stability and maneuverability [18, 61, 62].

In the fruit fly, the collapse in kinematic envelope may be quantified under tethered flight conditions in a closed-loop virtual reality flight simulator, in which the ability of the animal is scored to modulate stroke frequency and stroke amplitudes at different flight forces. In these experiments, the flies actively stabilize the azimuth velocity of a visual object (black bar) displayed in the panorama using the bilateral difference in stroke amplitude between both wings. While steering toward the visual target, the flies modulate *mean* stroke amplitude on both body sides in response to the up- and down motion of a superimposed, open-loop background pattern [22]. At maximum flight force production, the temporal deviation of stroke amplitude and frequency approaches zero, indicating that the animal is restricted to a unique combination of mean wing velocity (the product between amplitude and frequency) and mean lift coefficient (Fig. 17.4B,C) [62].

Ignoring the potential contribution of other kinematic parameters, this collapse of the kinematic envelope during peak force production should greatly attenuate maneuverability and stability of animals in free flight. A possible mechanism that helps small insects to remain stable around their roll and yaw axes at elevated force production is the wings' high-profile drag. As already outlined in the previous sections, even without any active control, frictional damping on the flapping wings is high enough to terminate yaw turning within 3–5 stroke cycles. Consequently, high frictional damping in the fruit fly helps to ensure stable flight conditions in cases in which force control by the neuromuscular system fails due to the mechanical limits of the thoracic box for wing motion.

17.4.2.3 Significance of Muscle Precision and Response Time of Sensory Feedback

Another parameter that limits stability and maneuverability is the muscular precision of the flight apparatus, including the temporal delay of sensory feedback. In Sect. 17.3.1 we discussed the relationship between moments of inertia, frictional damping on body and wings, turning velocity, and yaw torque production in a freely maneuvering insect. In terms of free flight stability and turning behavior, however, it is of interest to derive angular velocity for turning from Eq. (17.1). A time-variant form for yaw turning velocity at time t is

$$\omega(t) = \left[T(t) + \frac{I}{dt}\omega(t-1)\right] \Big/ \left[C + \frac{I}{dt}\right]. \quad (17.13)$$

Since torque production is proportional to the product of the bilateral difference instroke amplitude between both wings and an experimentally derived conversion factor (fruit fly: 2.9×10^{-10} Nm deg^{-1}) [61], we may link the ability of an insect to keep track during turning and to precisely steer toward a visual object to its temporal changes in stroke amplitude. In free flight, changes in stroke amplitude are due to the interplay between the mechano-sensory system (halteres, antennae, and campaniform sensilla), the visual system (compound eyes and ocelli), and the muscular system.

In contrast to insects with synchronous power muscles, such as dragonflies, in flies, power and control reside in two different muscle systems: the asynchronous indirect flight muscles (IFM) and the synchronous direct flight control muscles. IFM provide the power to overcome inertia and drag during wing flapping and fill up most of the thorax. By contrast, reconfiguration of the wing hinge for flight control lies in the function and interplay of 17 tiny flight control muscles. Flight control muscles typically produce positive work but also function as active springs that absorb mechanical muscle power produced by the IFM [63]. There is multiple electrophysiological evidence that three groups of control muscles play a key role in stroke amplitude control of flies: the basalare muscles b1–b3 and the muscles of the first (I1, I2) and third axillare (III1–4, Fig. 17.1B) [13–17, 64].

The flight control muscles in flies receive input from two major sensory organs: the gyroscopic halteres and the compound eyes. The halteres are condensed hindwings, driven by own power and flight control muscles [12]. Halteres beat in anti-phase with the wings and sense changes in Coriolis forces when the animal body rotates [10–12, 65]. They project on control muscle motoneurons via fast electrical synapses [66]. In fruit flies, halteres encode angular velocities

of up to at least 700° s^{-1} [67] during turning and provide fast feedback within at least a single wing stroke of approximately 5 ms [68]. By contrast, the vision system in insects suffers from a long delay scattered around 30 ms. The latter value was estimated from behavioral studies on male–female chases in houseflies, *Musca* [69]. Most of this delay appears to be due to the time-to-peak response of the photo-transduction process, i.e., 12 and 41 ms for the dark- and light-adapted state of the housefly's compound eye, respectively [70]. The values reported for fruit flies are similar to those of houseflies and range from 20 to 50 ms bump latency [71].

To incorporate the properties of the sensory feedback into our analytical framework, we may modify Eq. (17.1) by inserting the response time and the upper threshold for detecting rotational body movements by the sensory organs [5, 40]. Replacing the various terms, we obtain a time-invariant equation:

$$T_{Max} = I\omega_V/t_V + C\omega_V, \qquad (17.14)$$

in which ω_V is the limit of angular speed allowing the fly to determine its angular rotation, and the ratio ω_V/t_V is the maximum angular acceleration between the upper limit of the angular speed and the sensorimotor reaction time t_V of the fly.

Consequently, the term T_{Max} indicates the maximum torque allowed for heading stabilization during active flight control within the limits of the sensory apparatus.

Considering Eq. (17.14) from an evolutionary perspective, we may predict the following phenomenon: Insects exhibiting small delays in sensory information processing and large damping coefficients on wings and body reduce their need to develop a muscular system with high accuracy for wing motion, and thus high accuracy for yaw torque control. By contrast, a flight system with large response delays at small frictional damping requires a very precise muscular apparatus to avoid instabilities during flight. Understanding these trade-offs is of great relevance for the design of biomimetic micro-air vehicles that need to gain stability due to the function of both their electrical control circuitries and the actuators that drive wing flapping.

Surprisingly, in fruit flies flying at their natural frictional damping coefficient, vision-mediated flight requires very high precision of wing amplitude control for flight-heading stability within a range from 0.25° to 0.85° for each wing (Eq. (17.14), Fig. 17.9). Behavioral tests on tethered flies flying under vision-mediated closed-loop conditions in a flight simulator, however, show that the neuromuscular system is not able to control stroke amplitude below a threshold of 1–2° [40]. Consequently, the tethered animals fail to safely control yaw moments based on vision alone, suggesting additional feedback coming from the halteres in freely flying animals. However, a fruit fly exhibiting a 5 ms response time of the visual system (delay of a single stroke cycle) might keep instantaneous angular velocity of the body below the threshold of the visual system even at its natural damping coefficient, because the required changes in stroke amplitude for flight stabilization would range between 0.6° and 1.9° and would thus be within the scope of visually mediated yaw control. Nevertheless, despite the recent progress in understanding the feedback control cascade in flies, the exact contribution of each sensory system for force control in a freely cruising animal still needs to be determined.

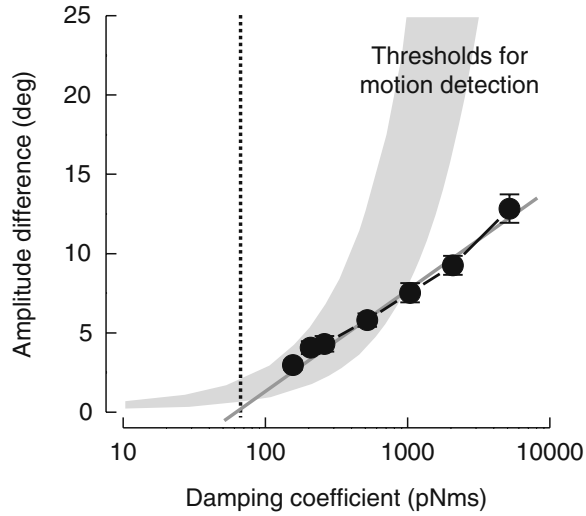

Fig. 17.9 Precision of steering control in tethered flying fruit flies. Data show the absolute difference between left- and right-wing stroke amplitude of flies (i.e., proportional to yaw torque), produced in order to actively stabilize yaw heading toward a black stripe displayed inside a flight simulator. The shaded area indicates the upper limits of the visual system that allow visual control of the stripe according to Eq. (17.14) (50 and 100% response thresholds of the insect's elementary motion detector, EMD). The dotted line indicates crossing of the regression line with the *x*-axis. Natural damping coefficient of the fruit fly amounts to 54 pNms. Means ± S.E. N= 47 flies. See also [40]

17.5 Synopsis

Heading toward the construction of robotic biomimetic micro-air vehicles based on flapping wing design is challenging (see other chapters in this book), and a detailed and integrative view on flight control in insects is thus of great interest. In this chapter, we focused on the interplay between the physical forces and the neuromuscular control cascade during yaw turning in a small fly. Our analysis shows that aerial behavior results from the *combined* properties of the flight feedback cascade, including the physiological limits of the nervous structures, the constraints on flight muscle function, and the physics of body dynamics during flight. Consequently, if we experimentally break the connection between the various functional hierarchies for flight control in an insect, we potentially face the risk that the system changes its locomotor state and our analyses are restricted to descriptions of functionally isolated sub-components of the flight apparatus. For example, if we ignore frictional damping during turning flight in *Drosophila*, we tempt to conclude that flight stability resides in a fast and very precise system for sensory information processing and wing control. By contrast, including passive stabilization of the insect body due to high frictional damping, the computational load on the central nervous system may decrease as well as the required speed of sensory information processing and the precision of wing control.

The ultimate challenge in understanding flight control and the limits of maneuverability, however, lies in the large variety of insect species and thus locomotor designs. A major goal for understanding both the biology of flight and the design of biomimetic micro-air vehicles must thus be to derive a *comprehensive* view on flapping flight that includes the various forms of senso-motor control. Eventually, this approach seems to be beneficial not only to evaluate the various forms of flight in insects but also to comprehend the physics and neuromuscular function of wing control in other flying animals, such as birds and bats.

References

1. Alexander, D.E. : Wind tunnel studies of turns by flying dragonflies. The Journal of Experimental Biology **122**, 81–98 (1986)
2. Ennos, A.R.: The kinematics and aerodynamics of the free flight of some Diptera. The Journal of Experimental Biology **142**, 49–85 (1989)
3. Fry, S.N., Sayaman, R., Dickinson, M.H.: The aerodynamics of free-flight maneuvers in *Drosophila*. Science **300**, 495–498 (2003)
4. Marden, J.H., Wolf, M.R., Weber, K.E.: Aerial performance of *Drosophila melanogaster* from populations selected for upwind flight ability. The Journal of Experimental Biology **200**, 2747–2755 (1997)
5. Mronz, M., Lehmann, F.-O.: The free flight response of *Drosophila* to motion of the visual environment. The Journal of Experimental Biology **211**, 2026–2045 (2008)
6. Rüppell, G.: Kinematic analysis of symmetrical flight manoeuvres of odonata. The Journal of Experimental Biology **144**, 13–42 (1989)
7. Wagner, H.: Flight performance and visual control of flight of the free-flying housefly (*Musca domestica*L) II Pursuit of targets. Philosophical Transactions of the Royal Society of London. Series B **312**, 553–579 (1986)
8. Wang, H., Zeng, L., Liu, H., Chunyong, Y.: Measuring wing kinematics, flight trajectory and body attitude during forward flight and turning maneuvers in dragonflies. The Journal of Experimental Biology **206**, 745–757 (2003)
9. Zbikowski, R.: Red admiral agility. Nature **420**, 615–618 (2002)
10. Nalbach, G.: The halteres of the blowfly *Calliphora* I kinematics and dynamics. Journal Comparative Physiology A **173**, 293–300 (1993)
11. Nalbach, G.: Extremely non-orthogonal axes in a sense organ for rotation: Behavioral analysis of the dipteran haltere system. Neuroscience **61**, 149–163 (1994)
12. Pringle, J.W.S.: The gyroscopic mechanism of the halteres of Diptera. Philosophical Transactions of the Royal Society of London. Series B **233**, 347–384 (1948)
13. Balint, C.N., Dickinson, M.H.: Neuromuscular control of aerodynamic forces and moments in the blowfly, *Calliphora vivina*. The Journal of Experimental Biology **207**, 3813–3838 (2004)
14. Dickinson, M.H., Lehmann, F.-O., Götz, K.G.: The active control of wing rotation by *Drosophila.* The Journal of Experimental Biology **182**, 173–189 (1993)
15. Dickinson, M.H., Lehmann, F.-O., Sane, S.: Wing rotation and the aerodynamic basis of insect flight. Science **284**, 1954–1960 (1999)
16. Götz, K.G., Hengstenberg, B., Biesinger, R.: Optomotor control of wing beat and body posture in *Drosophila*. Biol Cybernetics **35**, 101–112 (1979)
17. Heide, G.: Flugsteuerung durch nicht-fibrilläre Flugmuskeln bei der Schmeißfliege *Calliphora*. Z Vergl Physiologie **59**, 456–460 (1968)
18. Lehmann, F.-O., Dickinson, M.H.: The control of wing kinematics and flight forces in fruit flies (*Drosophila* spp). The Journal of Experimental Biology **201**, 385–401 (1998)
19. Casey, T.M., Ellington, C.P.: Energetics of insect flight. In: W. Wieser, E. Gnaiger (eds.) In Energy Transformations in Cells and Organisms, pp. 200–210. Stuttgart, Thieme (1989)
20. Harrison, J.F., Roberts, S.P.: Flight respiration and energetics. Annual Review of Physiology **62**, 179–205 (2000)

21. Lehmann, F.-O.: The constraints of body size on aerodynamics and energetics in flying fruit flies: an integrative view. Zoology **105**, 287–295 (2002)
22. Lehmann, F.-O., Dickinson, M.H.: The changes in power requirements and muscle efficiency during elevated force production in the fruit fly, *Drosophila melanogaster.* The Journal of Experimental Biology **200**, 1133–1143 (1997)
23. Borst, A., Egelhaaf, M.: Principles of visual motion detection. Trends in Neurosciences **12**, 297–306 (1989)
24. Dill, M., Wolf, R., Heisenberg, M.: Visual pattern recognition in *Drosophila* involves retinotopic matching. Nature **365**, 751–753 (1993)
25. Egelhaaf, M., Borst, A.: Motion computation and visual orientation in flies. Comparative Biochemistry and Physiology **104A**, 659–673 (1993)
26. Franceschini, N., Riehle, A., Nestour, A.: Directionally selective motion detection by insect neurons. In: Stavenga, Hardie (eds.) In Facets of vision, pp. 361–390. Berlin Heidelberg, Springer (1989)
27. Kirschfeld, K.: Automatic gain control in movement detection of the fly. Naturwissenschaften **76**, 378–380 (1989)
28. Krapp, H.G., Hengstenberg, B., Hengstenberg, R.: Dentritic structure and receptive-field organization of optic flow processing interneurons in the fly. American Physiological Society. Journal of Neurophysiology **79** 1902–1917 (1998)
29. O'Carroll, D.: Feature-detecting neurons in dragonflies. Nature **362** 541–543 (1993)
30. Reichardt, W.: Evaluation of optical motion information by movement detectors. Journal of Comparative Physiology A **161**, 533–547 (1987)
31. Tammero, L.F., Dickinson, M.H.: Spatial organization of visuomotor reflexes in *Drosophila.* The Journal of Experimental Biology **207**, 113–122 (2004)
32. Blondeau, J., Heisenberg, M.: The three dimensional optomotor torque system of *Drosophila melanogaster*. Journal of Comparative Physiology A **145**, 321–329 (1982)
33. Borst, A., Bahde, S.: Comparison between the movement detection systems underlying the optomotor and the landing response in the housefly. Biological Cybernetics **56**, 217–224 (1987)
34. Duistermars, B.J., Chow, D.M., Condro, M., Frye, M.A.: The spatial, temporal and contrast properties of expansion and rotation flight optomotor responses in *Drosophila.* The Journal of Experimental Biology **210**, 3218–3227 (2007)
35. Egelhaaf, M.: Visual afferences to flight steering muscles controlling optomotor responses of the fly. Journal of Comparative Physiology A **165**, 719–730 (1989)
36. Götz, K.G., Wandel, U.: Optomotor control of the force of flight in *Drosophila* and *Musca* II Covariance of lift and thrust in still air. Biological Cybernetics **51**, 135–139 (1984)
37. Heide, G., Götz, K.G.: Optomotor control of course and altitude in *Drosophila* is achieved by at least three pairs of flight steering muscles. The Journal of Experimental Biology **199,** 1711–1726 (1996)
38. Heisenberg, M., Wolf, R.: Reafferent control of optomotor yaw torque in *Drosophila melanogaster.* Journal of Comparative Physiology A **163**, 373–388 (1988)
39. Kaiser, W., Liske, E.: Die optomotorischen Reaktionen von fixiert fliegenden Bienen bei Reizung mit Spektrallichtern. Journal of Comparative Physiology **80**, 391–408 (1974)
40. Hesselberg, T., Lehmann, F.-O.: Turning behaviour depends on frictional damping in the fruit fly *Drosophila.* The Journal of Experimental Biology **210**, 4319–4334 (2007)
41. Schilstra, C., van Hateren, J.H.: Blowfly flight and optic flow I. Thorax kinematics and flight dynamics. The Journal of Experimental Biology **202**, 1481–1490 (1999)
42. Egelhaaf, M., Borst, A.: Is there a separate control system mediating a "centering response" in honeybees. Naturwissenschaften **79**, 221–223 (1992)
43. Srinivasan, M.V., Lehrer, M., Kirchner, W.H., Zhang, S.W.: Range perception through apparent image speed in freely flying honey bees. Visual Neuroscience **6**, 519–535 (1991)
44. Ennos, A.R.: The kinematics and aerodynamics of the free flight of some Diptera. The Journal of Experimental Biology **142**, 49–85 (1989)
45. Hedrick, T.L., Usherwood, J.R., Biewener, A.A.: Low speed maneuvering flight of the rose-breasted cockatoo (*Eolophus roseicapillus*) II Inertial and aerodynamic reorientation. The Journal of Experimental Biology **210**, 1912–1924 (2007)
46. Ellington, C.P.: The aerodynamics of insect flight VI Lift and power requirements. Philosophical Transactions of the Royal Society of London. Series B **305**, 145–181 (1984)
47. Ramamurti, R., Sandberg, W.C.: A computational investigation of the three-dimensional unsteady aerodynamics of *Drosophila* hovering and maneuvering. The Journal of Experimental Biology **210**, 881–896 (2007)
48. Heisenberg, M., Wolf, R.: Vision in *Drosophila*. Springer-Verlag, Berlin (1984)
49. Ramamurti, R., Sandberg, W.C.: Computational study of 3-D flapping foil flows 39th Aerospace Sciences Meeting and Exhibit, 605 (2001)
50. David, C.T.: The relationship between body angle and flight speed in free flying *Drosophila*. Physiological Entomology **3**, 191–195 (1978)
51. Marden, J.H.: Maximum lift production during take-off in flying animals. The Journal of Experimental Biology **130**, 235–258 (1987)
52. Roeder, K.D., Treat, A.E.: The detection and evasion of bats by moths. Am Sci **49**, 135–148 (1961)
53. Almbro, M., Kullberg, C.: Impaired escape flight ability in butterflies due to low flight muscle ratio prior to hibernation. The Journal of Experimental Biology **211**, 24–28 (2008)
54. Marden, J.H., Fitzhugh, G.H., Wolf, M.R.: From molecules to mating success: Integrative biology of muscle maturation in a dragonfly. American Scientist **38**, 528–544 (1998)
55. Barton, B., Ayer, G., Heymann, N., Maughan, D.W., Lehmann, F.-O., Vigoreaux, J.O.: Flight muscle properties and aerodynamic performance of *Drosophila* expressing a *flightin* gene. The Journal of Experimental Biology **208**, 549–560 (2005)
56. Norberg, R.A.: Hovering flight of the dragonfly *Aeshna juncea* L. In: T.Y.-T. Wu, C.J. Brokaw, C. Brennen (eds.) Kinematics and Aerodynamics, vol. 2, pp. 763–781. NY, Plenum Press (1975)
57. Reavis, M.A., Luttges, M.W.: Aerodynamic forces produced by a dragonfly. AIAA Journal **88**:**0330**, 1–13 (1988)

58. Wakeling, J.M., Ellington, C.P.: Dragonfly Flight II. Velocities, accelerations, and kinematics of flapping flight. The Journal of Experimental Biology **200**, 557–582 (1997)
59. Usherwood, J.R., Lehmann, F.-O.: Phasing of dragonfly wings can improve aerodynamic efficiency by removing swirl. Journal of the Royal Society, Interface **5**, 1303–1307 (2008)
60. Thomas, A.L.R, Taylor, G.K., Srygley, R.B., Nudds, R.L., Bomphrey, R.J.: Dragonfly flight: Free-flight and tethered flow visualizations reveal a diverse array of unsteady lift-generating mechanisms, controlled primarily via angle of attack. The Journal of Experimental Biology **207**, 4299–4323 (2004)
61. Götz, K.G.: Bewegungssehen und Flugsteuerung bei der Fliege *Drosophila.* In: W. Nachtigall (ed.) BIONA-report 2 Fischer, Stuttgart (1983)
62. Lehmann, F.-O., Dickinson, M.H.: The production of elevated flight force compromises flight stability in the fruit fly *Drosophila*. The Journal of Experimental Biology **204**, 627–635 (2001)
63. Tu, M.S., Dickinson, M.H.: Modulation of negative work output from a steering muscle of the blowfly *Calliphora vicina.* The Journal of Experimental Biology **192**, 207–224 (1994)
64. Lehmann, F.-O., Götz, K.G.: Activation phase ensures kinematic efficacy in flight-steering muscles of *Drosophila melanogaster*. Journal Comparative Physiology **179**, 311–322 (1996)
65. Nalbach, G., Hengstenberg, R.: The halteres of the blowfly *Calliphora* II Three-dimensional organization of compensatory reactions to real and simulated rotations. Journal Comparative Physiology A **174**, 695–708 (1994)
66. Fayyazuddin, A., Dickinson, M.H.: Haltere afferents provide direct, electronic input to a steering motor neuron of the blowfly, *Calliphora.* Journal of Neuroscience **16**, 5225–5232 (1996)
67. Sherman, A., Dickinson, M.H.: A comparison of visual and haltere-mediated equilibrium reflexes in the fruit fly *Drosophila melanogaster.* The Journal of Experimental Biology **206**, 295–302 (2003)
68. Hengstenberg, R., Sandeman, D.C.: Compensatory head roll in the blowfly *Calliphora* during flight. Proceedings of the Royal Society of London. Series B **227**, 455–482 (1986)
69. Land, M.F., Collett, T.S.: Chasing Behaviour of houseflies (*Fannia canicularis*). Journal of Comparative Physiology A **89**, 331–357 (1974)
70. Howard, J., Dubs, A., Payne, R.: The dynamics of phototransduction in insects: A comparative study. Journal of Comparative Physiology A **154,** 707–718 (1984)
71. Hardie, C.R., Raghu, P.: Visual transduction in *Drosophila.* Nature **413**, 186–193 (2001)